NUMERICAL TREATMENT OF AQUATIC VEGETATION

Hye Keun Lee

Korea Water Resources Corporation, Taejon, Korea

Abstract: The presence of the vegetation causes damping of the wind, wave and current fields. To provide realistic simulation of wind-driven circulation in the presence of vegetation, this study developed a simplified vegetation model which parameterizes the effect of vegetation in terms of added "form drag" terms in the momentum equations.

Key Words: vegetation, circulation, curvilinear, lake

1. INTRODUCTION

The western portion of Lake Okeechobee, florida, U.S.A, is covered with an extensive amount of vegetation. The vegetation can affect the circulation in several different ways. First of all, wind stress over the emergent vegetation is reduced below that over the open water. Furthermore, the submerged vegetation introduces drag force to the water column. Because most of the vegetation stalks are elongated cylinders without large leaf areas, the drag force is primarily associated with the profile drag (or form drag) instead of the skin friction drag. The profile drag can reduce the flow and is proportional to the "projected area" of vegetation in the direction of the flow.

The presence of vegetation also can affect the turbulence in the water column. The characteristic sizes of the horizontal and vertical eddies are generally reduced by the vegetation. This usually leads to a reduction of turbulence, although some wake turbulence may be generated on the downstream side of vegetation.

In order to simulate the effects of vegetation, several approaches have been undertaken in previous investigations. For example, Saville (1952) and Sheng et al. (1991) used an empirical correction factor to simulate the reduction of wind stress over the vegetation area. Sheng et al. (1991) also adjusted the bottom friction coefficient over the vegetation area. For simplicity, however, Sheng et al. did not include the effect of vegetation on mean flow and turbulence in the water column, because the primary focus of that study was the internal loading of nutrients from the bottom sediments in the open water zone. Whitaker et al. (1975) developed a two-dimensional, vertically-integrated model of storm surges in Lake Okeechobee. The profile drag created by the vegetation was included in the linearized vertically-integrated equations of motion, which did not contain the nonlinear and diffusion terms. Sheng (1982) developed a

comprehensive model of turbulent flow over vegetation canopy by considering both the profile drag and the skin friction drag in the momentum equations in addition to the reduction of turbulent eddies and the creation of turbulent wake energy. Detailed vertical structures of mean flow and turbulence stresses were computed by solving the dynamic equations of all the mean flow and turbulent quantities. Model results compared well with available mean flow and turbulence data in a vegetation zone.

For the present study, due to the lack of detailed data on vegetation and mean flow and turbulence in the vegetation zone, a relatively simple vegetation model which is more robust than Whittaker et al.'s model yet simpler than Sheng's 1982 model is developed. Due to the shallow depth in the vegetation zone, it is feasible to treat the water column with no more than two vertical layers. When the height of vegetation is greater than 80% of the total water depth, the flow is considered to be one-layer flow, i.e., the entire water column is considered to contain uniformly distributed vegetation. When the height of vegetation is between 20% and 80% of the total water depth, the flow is considered to be two-layer flow, i.e., the water column consists of a water layer on top of a vegetation layer. The vegetation effect is neglected when the height of vegetation is less than 20% of the total depth. The profile drag introduced by the vegetation can be formulated in the form of a quadratic stress law:

$$\bar{\tau}_{canopy} = \rho\ c_d \bar{u}_1 |\bar{u}_1|\, AN \qquad (1)$$

where u is the vertically averaged velocity in the vegetation layer (layer 1), ρ is the density of water, A is the projected area of vegetation in the direction of the flow, N is the number of stalks per unit horizontal area, and c_d is an empirical drag coefficient. Tickner (1957) performed a laboratory study. Strips of ordinary window screen 0.1 foot in height were placed across a channel to simulate a vegetative canopy. Using Tickner's experimental results, Whitaker et al. (1975) calculated c_d (1.77) which was used in this study. Roig and King (1992) showed c_d is a function of Froude Number, Reynolds Number, vegetation height, spacing, and diameter of vegetation. As the water level changes, the flow regime over a vegetation area may change from one-layer to two-layer flow, and vice versa.

2. GOVERNING EQUATIONS

Let us consider an (x, y, z) coordinate system with the velocity components in the (x, y, z) directions as (u, v, w). The lower layer (layer I) of the water column is covered with vegetation, while the upper layer (layer II) is vegetation-free (Fig. 1).

Flow in the vegetation layer (u_1, v_1) and flow in the vegetation-free layer (u_2, v_2) both satisfy the equations of motion.

Equations for the Vegetation Layer (Layer I)

$$\frac{\partial u_1}{\partial t} + \frac{\partial u_1^2}{\partial x} + \frac{\partial u_1 v_1}{\partial y} + \frac{\partial u_1 w_1}{\partial z} = fv_1 - \frac{1}{\rho}\frac{\partial p_1}{\partial x} + \frac{\partial}{\partial x}\left[A_H \frac{\partial u_1}{\partial x}\right] + \frac{\partial}{\partial y}\left[A_H \frac{\partial u_1}{\partial y}\right] + \frac{\partial}{\partial z}\left[A_v \frac{\partial u_1}{\partial z}\right] \qquad (2)$$

$$\frac{\partial v_1}{\partial t} + \frac{\partial u_1 v_1}{\partial x} + \frac{\partial v_1^2}{\partial y} + \frac{\partial v_1 w_1}{\partial z} = -fu_1 - \frac{1}{\rho}\frac{\partial p_1}{\partial y} + \frac{\partial}{\partial x}\left[A_H \frac{\partial v_1}{\partial x}\right] + \frac{\partial}{\partial y}\left[A_H \frac{\partial v_1}{\partial y}\right] + \frac{\partial}{\partial z}\left[A_v \frac{\partial v_1}{\partial z}\right] \qquad (3)$$

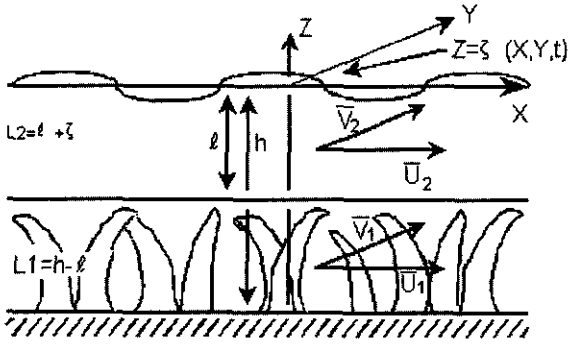

Fig. 1. Schematics of flow in vegetation zone

$$\frac{\partial p_1}{\partial y} = -\rho g \tag{4}$$

Integrating Equation (4) vertically:

$$p = p_a + \rho g(\varsigma - z) \tag{5}$$

Integrating Equations (2) and (3) vertically from $z=-h$ to $z=-l$:

$$\frac{\partial U_1}{\partial t} + \frac{\partial}{\partial x}\left(\frac{U_1^2}{L_1}\right) + \frac{\partial}{\partial y}\left(\frac{U_1 V_1}{L_1}\right) + gL_1\varsigma_x = fV_1 + \frac{1}{\rho}(\tau_{ix} - \tau_{bx} - F_{cx}) + \frac{\partial}{\partial x}\left[A_H \frac{\partial U_1}{\partial x}\right] + \frac{\partial}{\partial y}\left[A_H \frac{\partial U_1}{\partial y}\right] \tag{6}$$

$$\frac{\partial V_1}{\partial t} + \frac{\partial}{\partial x}\left(\frac{U_1 V_1}{L_1}\right) + \frac{\partial}{\partial y}\left(\frac{V_1^2}{L_1}\right) + gL_1\varsigma_y = -fU_1 + \frac{1}{\rho}(\tau_{iy} - \tau_{by} - F_{cy}) + \frac{\partial}{\partial x}\left[A_H \frac{\partial V_1}{\partial x}\right] + \frac{\partial}{\partial y}\left[A_H \frac{\partial V_1}{\partial y}\right] \tag{7}$$

where $L_1=h-l$ and U_1 and V_1 are the vertically-integrated velocities within the vegetation layer:

$$(U_1, V_1) \equiv \int_{-h}^{l} (u_1, v_1) dz \tag{8}$$

τ_{bx} and τ_{by} are bottom stresses, τ_{ix} and τ_{iy} are interfacial stresses between layer I and layer II, and F_{cx} and F_{cy} are form drags due to the vegetation canopy.

Equations for the Vegetation-Free Layer (Layer II)

$$\frac{\partial u_2}{\partial t} + \frac{\partial u_2^2}{\partial x} + \frac{\partial u_2 v_2}{\partial y} + \frac{\partial u_2 w_2}{\partial z} = fv_2 - \frac{1}{\rho}\frac{\partial p_2}{\partial x} + \frac{\partial}{\partial x}\left[A_H \frac{\partial u_2}{\partial x}\right] + \frac{\partial}{\partial y}\left[A_H \frac{\partial u_2}{\partial y}\right] + \frac{\partial}{\partial z}\left[A_v \frac{\partial u_2}{\partial z}\right] \tag{9}$$

$$\frac{\partial v_2}{\partial t} + \frac{\partial u_2 v2}{\partial x} + \frac{\partial v_2^2}{\partial y} + \frac{\partial v_2 w_2}{\partial z} = -fu_2 - \frac{1}{\rho}\frac{\partial p_2}{\partial y} + \frac{\partial}{\partial x}\left[A_H \frac{\partial v_2}{\partial x}\right] + \frac{\partial}{\partial y}\left[A_H \frac{\partial v_2}{\partial y}\right] + \frac{\partial}{\partial z}\left[A_v \frac{\partial v_2}{\partial z}\right] \tag{10}$$

Integrating Equation (9) and (10) vertically from $z=-l$ to $z=-\varsigma$ and defining $L_2 = l + \varsigma$:

$$\frac{\partial U_2}{\partial t} + \frac{\partial}{\partial x}\left(\frac{U_2^2}{L_2}\right) + \frac{\partial}{\partial y}\left(\frac{U_2 V_2}{L_2}\right) + gL_2\varsigma_x = fV_2 + \frac{1}{\rho}(\tau_{sx} - \tau_{ix}) + \frac{\partial}{\partial x}\left[A_H \frac{\partial U_2}{\partial x}\right] + \frac{\partial}{\partial y}\left[A_H \frac{\partial U_2}{\partial y}\right] \tag{11}$$

$$\frac{\partial V_2}{\partial t}+\frac{\partial}{\partial x}\left(\frac{U_2V_2}{L_2}\right)+\frac{\partial}{\partial y}\left(\frac{V_2^2}{L_2}\right)+gL_2\varsigma_y=-fU_2 +\frac{1}{\rho}(\tau_{sy}-\tau_{iy}) +\frac{\partial}{\partial x}\left[A_H\frac{\partial V_2}{\partial x}\right]+\frac{\partial}{\partial y}\left[A_H\frac{\partial V_2}{\partial y}\right] \quad (12)$$

where U_2 and V_2 are the vertically-integrated velocities within the vegetation-free layer:

$$(U_2,V_2)\equiv\int_{-l}^{\xi}(u_2,v_2)dz \quad (13)$$

Equations for the Entire Water Column

Instead of solving the above equations for the vegetation layer and the vegetation-free layer, it is more convenient to solve the vertically - integrated equations for the entire water column, which can be readily derived by combining the equations for the two layers. First, the vertically-integrated velocities over the entire water column in the vegetation zone, U and V, can be defined as

$$(U,V)\equiv(U_1+U_2,V_1+V_2)=(L_1\overline{u}_1+L_2\overline{u}_2,L_1\overline{v}_1+L_2\overline{v}_2) \quad (14)$$

where $\overline{u}_1$, $\overline{u}_2$, $\overline{v}_1$ and $\overline{v}_2$ are vertically - averaged velocities within layer I and layer II, respectively, while L_1 and L_2 are the thicknesses of layer I and layer II, respectively.

Adding the U_1 equation and the U_2 equation leads to

$$\frac{\partial U}{\partial t}+\frac{\partial}{\partial x}\left(\frac{U_1^2}{L_1}+\frac{U_2^2}{L_2}\right)+\frac{\partial}{\partial y}\left(\frac{U_1V_1}{L_1}+\frac{U_2V_2}{L_2}\right)+gH\varsigma_x=fV +\frac{1}{\rho}(\tau_{sx}-\tau_{bx}-F_{cx}) +\frac{\partial}{\partial x}\left[A_H\frac{\partial U}{\partial x}\right]+\frac{\partial}{\partial y}\left[A_H\frac{\partial U}{\partial y}\right] \quad (15)$$

while the summation of the V_1 equation and the V_2 equation results in

$$\frac{\partial V}{\partial t}+\frac{\partial}{\partial x}\left(\frac{U_1V_1}{L_1}+\frac{U_2V_2}{L_2}\right)+\frac{\partial}{\partial y}\left(\frac{V_1^2}{L_1}+\frac{V_2^2}{L_2}\right)+gH\varsigma_y=-fU +\frac{1}{\rho}(\tau_{sy}-\tau_{by}-F_{cy}) +\frac{\partial}{\partial x}\left[A_H\frac{\partial V}{\partial x}\right]+\frac{\partial}{\partial y}\left[A_H\frac{\partial V}{\partial y}\right] \quad (16)$$

All the stress terms are computed as the quadratic power of the flow velocity. For example, τ_{sx} and τ_{sy} are computed as quadratic functions of the wind speed, τ_{bx} and τ_{bx} are computed as quadratic functions of U and V, and τ_{ix} and τ_{iy} are quadratic functions of (U_2-U_1) and (V_2-V_1). The form drags associated with the vegetation are:

$$F_{cx}=\rho\ c_dA_xN_x\frac{\sqrt{U_1^2+V_1^2}}{L_1}\left(\frac{U_1}{L_1}\right) \quad (17)$$

$$F_{cx}=\rho\ c_dA_yN_y\frac{\sqrt{U_1^2+V_1^2}}{L_1}\left(\frac{V_1}{L_1}\right) \quad (18)$$

$$\tau_{ix}=\rho c_{di}\sqrt{\left(\frac{U_2}{L_2}-\frac{U_1^2}{L_1}\right)+\left(\frac{V_2}{L_2}-\frac{V_1}{L_1}\right)^2}\left(\frac{U_2}{L_2}-\frac{U_1}{L_1}\right) \quad (19)$$

$$\tau_{iy}=\rho c_{di}\sqrt{\left(\frac{U_2}{L_2}-\frac{U_1^2}{L_1}\right)+\left(\frac{V_2}{L_2}-\frac{V_1}{L_1}\right)^2}\left(\frac{V_2}{L_2}-\frac{V_1}{L_1}\right) \quad (20)$$

where c_d and c_{di} are empirical drag coefficients.

An additional equation that must be satisfied is the continuity equation:

$$\frac{\partial\varsigma}{\partial t}+\frac{\partial U}{\partial x}+\frac{\partial V}{\partial y}=0 \quad (21)$$

Dimensionless Equations in Curvilinear Grids

The above dimensional equations were presented to illustrate the development of the vegetation model. In the curvilinear-grid model, however, dimensionless equations in curvilinear grids are solved. These dimensionless equations are presented in the following in terms of the contravariant velocity components in two layers(Lee, 1993):

$$\frac{\partial U_1^{\xi}}{\partial t} + L_1\left[g^{11}\varsigma_{\xi} + g^{12}\varsigma_{\eta}\right] = \frac{g_{12}}{\sqrt{g_0}}U_1^{\xi} + \frac{g_{22}}{\sqrt{g_0}}U_1^{\eta} + \tau_{i\xi}^{*} - \tau_{b\xi}^{*} - F_{c\xi}^{*} + (HorizontalDiffusion)_{\xi}(U_1^{\xi}, U_1^{\eta}) + \frac{R_o}{L_1}\left[NonlinearTerms(U_1^{\xi}, U_1^{\eta})\right] \tag{22}$$

$$\frac{\partial U_1^{\eta}}{\partial t} + L_1\left[g^{21}\varsigma_{\xi} + g^{22}\varsigma_{\eta}\right] = -\frac{g_{11}}{\sqrt{g_0}}U_1^{\xi} - \frac{g_{21}}{\sqrt{g_0}}U_1^{\eta} + \tau_{i\eta}^{*} - \tau_{b\eta}^{*} - F_{c\eta}^{*} + (HorizontalDiffusion)_{\eta}(U_1^{\xi}, U_1^{\eta}) + \frac{R_o}{L_1}\left[NonlinearTerms(U_1^{\xi}, U_1^{\eta})\right] \tag{23}$$

$$\frac{\partial U_2^{\xi}}{\partial t} + L_2\left[g^{11}\varsigma_{\xi} + g^{12}\varsigma_{\eta}\right] = \frac{g_{12}}{\sqrt{g_0}}U_2^{\xi} + \frac{g_{22}}{\sqrt{g_0}}U_2^{\eta} + \tau_{s\xi}^{*} - \tau_{i\xi}^{*} + (HorizontalDiffusion)_{\xi}(U_2^{\xi}, U_2^{\eta}) + \frac{R_o}{L_2}\left[NonlinearTerms(U_2^{\xi}, U_2^{\eta})\right] \tag{24}$$

$$\frac{\partial U_2^{\eta}}{\partial t} + L_2\left[g^{21}\varsigma_{\xi} + g^{22}\varsigma_{\eta}\right] = -\frac{g_{11}}{\sqrt{g_0}}U_2^{\xi} - \frac{g_{21}}{\sqrt{g_0}}U_2^{\eta} + \tau_{s\eta}^{*} - \tau_{i\eta}^{*} + (HorizontalDiffusion)_{\eta}(U_2^{\xi}, U_2^{\eta}) + \frac{R_o}{L_2}\left[NonlinearTerms(U_2^{\xi}, U_2^{\eta})\right] \tag{25}$$

where

$$\tau_{s\xi}^{*} = \xi_x\tau_{sx}^{*} + \xi_y\tau_{sy}^{*} \tag{26}$$

$$\tau_{s\eta}^{*} = \eta_x\tau_{sx}^{*} + \eta_y\tau_{sy}^{*} \tag{27}$$

$$\tau_{i\xi}^{*} = \xi_x\left[\frac{\tau_{ix}}{\rho f U_r Z_r}\right] + \xi_y\left[\frac{\tau_{iy}}{\rho f U_r Z_r}\right] \tag{28}$$

$$\tau_{i\eta}^{*} = \eta_x\left[\frac{\tau_{ix}}{\rho f U_r Z_r}\right] + \eta_y\left[\frac{\tau_{iy}}{\rho f U_r Z_r}\right] \tag{29}$$

$$F_{c\xi}^{*} = \xi_x\left[\frac{F_{cx}}{\rho f U_r Z_r}\right] + \xi_y\left[\frac{F_{cy}}{\rho f U_r Z_r}\right] \tag{30}$$

$$F_{c\eta}^{*} = \eta_x\left[\frac{F_{cx}}{\rho f U_r Z_r}\right] + \eta_y\left[\frac{F_{cy}}{\rho f U_r Z_r}\right] \tag{31}$$

Defining

$$U^{\xi} = U_1^{\xi} + U_2^{\xi} \tag{32}$$

$$U^{\eta} = U_1^{\eta} + U_2^{\eta} \tag{33}$$

we can obtain the following equations for the entire water column:

$$\frac{\partial U^{\xi}}{\partial t} + H\left[g^{11}\varsigma_{\xi} + g^{12}\varsigma_{\eta}\right] = \frac{g_{12}}{\sqrt{g_0}}U^{\xi} + \frac{g_{22}}{\sqrt{g_0}}U^{\eta} + \tau_{s\xi}^{*} - \tau_{b\xi}^{*} - F_{c\xi}^{*} + (HorizontalDiffusion)_{\xi}(U_1^{\xi}, U_1^{\eta}) + (HorizontalDiffusion)_{\xi}(U_2^{\xi}, U_2^{\eta}) + \frac{R_o}{L_1}\left[NonlinearTerms(U_1^{\xi}, U_1^{\eta})\right] + \frac{R_o}{L_2}\left[NonlinearTerms(U_2^{\xi}, U_2^{\eta})\right] \tag{34}$$

$$\frac{\partial U^{\eta}}{\partial t} + H\left[g^{21}\varsigma_{\xi} + g^{22}\varsigma_{\eta}\right] \tag{35}$$

$$= -\frac{g_{11}}{\sqrt{g_0}}U^{\xi} - \frac{g_{21}}{\sqrt{g_0}}U^{\eta} + \tau^*_{s\eta} - \tau^*_{b\eta} - F^*_{c\eta}$$
$$+ (HorizontalDiffusion)_{\eta}(U_1^{\xi}, U_1^{\eta})$$
$$+ (HorizontalDiffusion)_{\eta}(U_2^{\xi}, U_2^{\eta})$$
$$+ \frac{R_o}{L_1}\left[NonlinearTerms(U_1^{\xi}, U_1^{\eta})\right]$$
$$+ \frac{R_o}{L_2}\left[NonlinearTerms(U_2^{\xi}, U_2^{\eta})\right]$$

The dimensionless continuity equation in the curvilinear grids becomes:

$$\varsigma_t + \frac{\beta}{\sqrt{g_o}}\left[\frac{\partial}{\partial\xi}\left(\sqrt{g_o}U^{\xi}\right) + \frac{\partial}{\partial\eta}\left(\sqrt{g_o}U^{\eta}\right)\right] = 0 \qquad (36)$$

3. VEGETATION PARAMETERS

The distribution of aquatic vegetation in Lake Okeechobee was determined by the use of recent satellite imageries and ground truth data obtained during field surveys. Satellite imageries from the SPOT satellite were received and processed to create a vegetation map of Lake Okeechobee (Richardson, J. R., personal communication, 1991). This map was overlayed onto a curvilinear grid. The number of pixels with the same color was counted to classify the vegetation type on each grid cell. The vegetation data include the vegetation class, the height of vegetation, the number of stalks per unit area, and the diameter of each class. A total of more than 25 kinds of vegetation were identified. The range of vegetation height is between 0.5 m and 4 m. The density ranges from 10 stalks per m^2 to 2000 stalks per m^2 of bottom area, while the diameter of the stalks ranges from 0.25 cm to 15 cm. The most popular type of vegetation was cattail.

Each type of vegetation has a different diameter and height. For simplicity, in this study it was assumed that all types of vegetation have cylindrical stalks. Table 1 shows the various types of vegetation found in Lake Okeechobee.

To represent the vegetation distribution accurately, the concept of "equivalent vegetation density" is introduced. The equivalent vegetation density is defined as the equivalent number of stalks with 1 cm diameter per unit horizontal area which will give the same total "projected area." If, however, the effect of skin friction drag due to vegetation is more important, then the "equivalent vegetation density" has to be defined in terms of the total "wetted area" rather than the total "projected area." The procedure for incorporating the vegetation information into our model is described as follows.

Let

d_i = the diameter of the i-th vegetation type [cm],

ρ_i = the number of stalks of the i-th vegetation type per unit area,

h_i = the height of the i-th vegetation type in the grid cell [m],

D = the average water depth in the grid cell [m],

A = the total area of the grid cell [m^2], and

P_i = the percent area occupied by the i-th vegetation type within the total area of the grid cell

The sum of the heights of all the plants in the grid cell, H, is

$$H = \sum_i \rho * h_i * P_i / 100 * A \qquad (37)$$

and the total number of stalks of the plants in the grid cell, T, is

$$T = \sum_i \rho_i * P_i / 100 * A \qquad (38)$$

whereupon the average height of vegetation in

Table 1. Vegetations in Lake Okeechobee (From Richardson, 1991)

Value	Points	Acres	%	Height [m]	Density [$\#/m^2$]	Diameter [m]	Description
0	41631	38228.64	0				
1	36	33.058	0.01	2.5	10	2	Buttonbush
2	2737	2513.315	0.57	4	30	8	Melaleuca
3	5699	5233.241	1.18	2.5	10	5	Willow
4	43	39.486	0.01	1	2000	0.25	Spartina
5	43433	39883.37	9.03	2.5	50	7	Cattail
6	3975	3650.138	0.83	1.5	40	15	Sawgrass
7	1195	1097.337	0.25	5	10	2	Mixed Upland
8	4712	4326.905	0.98	1	500	0.25	Rhynchospora
9	36	33.058	0.01	0.5	10	1	Sagitaria/pontedaria
10	11458	10521.57	2.38	1	2000	0.25	Mixed grasses
11	1316	1208.448	0.27	0	7	1	Nymphae
12	6836	6277.318	1.42	1	60	0.25	Eleocharis
13	36	33.058	0.01	5	10	2	Guava
14	44	40.404	0.01	0	100	5	Hyacinth
15	4029	3699.724	0.84	2.5	50	2	Scirpus
16	370750	340449.9	77.08	0	0	0	Open Water
17	196	179.982	0.04	0	0	0	Periphyton
18	5344	4907.254	1.11	1	100	0.25	Eleocharis/periphyton mix
19	2365	2171.717	0.49	1	100	0.3	Nymphae/eleocharis mix
20	2759	2533.517	0.57	0.5	15	3.5	Lotus
21	2238	2055.096	0.47	0	*	*	Submerged
22	2724	2501.377	0.57	2	12	5	Cattail/nymphae mix
23	714	655.647	0.15	2.5	50	5	Phragmites
24	278	255.28	0.06	1	50	0.3	Maidencane
25	3952	3629.017	0.82	**	**	**	Excluded
26	873	801.653	0.18	1	2000	0.25	Spartina/panicum mix
27	30	27.548	0.01	0	0	0	Airboat trails
28	3181	2921.028	0.66	1	100	1	Successional disturbed

1 * provides no wind resistance but considerable cross section resistance to flow
2 ** area diked preventing surface water flow

the grid cell, H_{canopy}, is

$$H_{canopy} = H / T \tag{39}$$

The distribution of H_{canopy}, in Lake Okeechobee determined by this method is shown in Fig. 2.

The projected area occupied by the i-th vegetation type in the grid cell is

$$\alpha_i = \rho_i * d_i * h_i * P_i / 100 * A \tag{40}$$

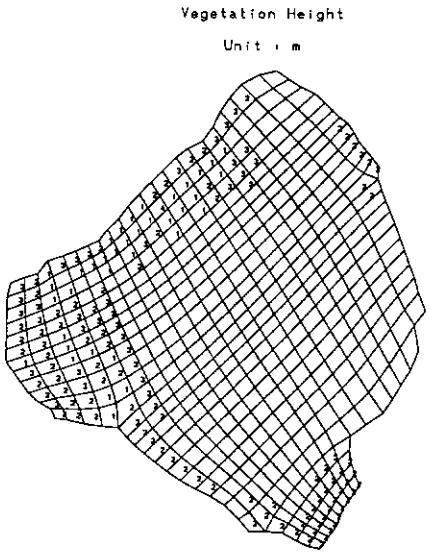

Fig. 2. Distribution of vegetation height in Lake Okeechobee

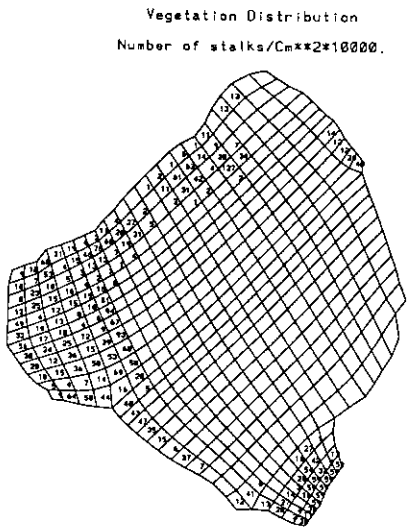

Fig. 3. Distribution of vegetation density in Lake Okeechobee

and the total projected area occupied by plants in the cell is

$$S = \sum_i \alpha_i \tag{41}$$

whereupon the equivalent vegetation density is

$$N = S/(A * H_{canopy} * D_{canopy}) \tag{42}$$

where d_i is assumed to be 1 cm. However, if we assume the height of each vegetation type is the same as average water depth in the cell, h_i is replaced by D in Equation 40 and H_{canopy} is replaced by D in Equation 42. The distribution of N in Lake Okeechobee is shown in Fig. 3.

The value of the profile drag coefficient for a cylinder, c_d, was set to be 1.77 in this study. Whitaker et al.(1975) estimated the interfacial stress coefficient, c_{di}, by calibrating the one-dimensional surge model with the observed quasi steady-state surface profile in Lake Okeechobee.

4. APPLICATION TO LAKE OKEECHOBEE

Lake Okeechobee, located between latitudes 27°×12′ N and 26°×40′ N and longitudes 80°×37′ W and 81°×08′W, is the largest freshwater lake in America, exclusive of the Great Lakes. With an average depth of approximately 3m, and the deepest part less than 5m deep, the basin is shaped like a very shallow saucer. The western part of the lake contains a great deal of emergent and submerged vegetation. According to satellite photos, marsh constitutes 24% of the lake surface area.

During the fall of 1988 and the spring of 1989, field data were collected by the Coastal and Oceanographic Engineering Department, University of Florida. Six platforms were set up in Lake Okeechobee. Measured data at these six platforms include wind, current, water temperature, wave, and turbidity. In this study, wind data

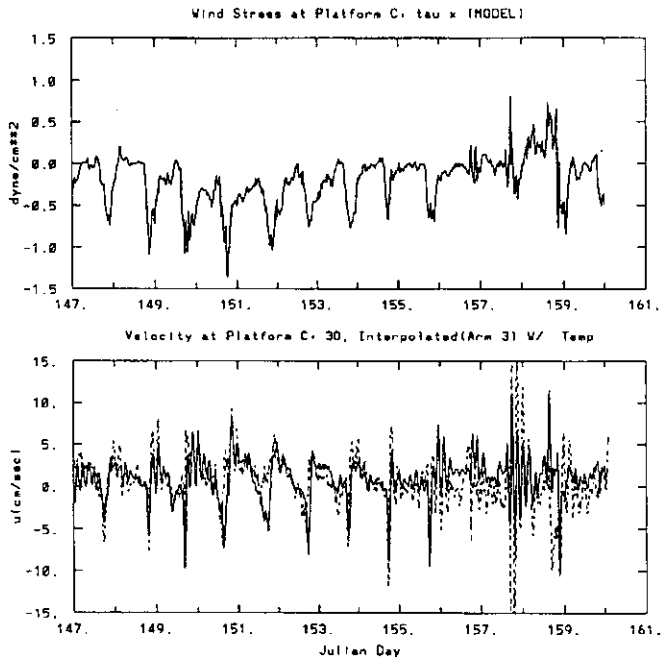

Fig. 4. Simulated (solid lines) and measured (dotted lines) currents at Station C (Arm 3: East-West direction)

were used to compute the wind stress field, which is an essential boundary condition for the simulation of the wind-driven circulation. Current data were used to calibrate and validate the 3-D hydrodynamics model.

The first step for simulation is to select the grid and grid size. Rectangular Cartesian grids were widely used in hydrodynamic models. These grids are easy to generate but have a disadvantage.

Because these grids have to represent the boundaries in a stair-stepped fashion, they cannot represent the complex geometry accurately unless a large number of grid points are used.

Complex boundaries can be represented more accurately by using the curvilinear grid for a general 2-D region with boundaries of arbitrary shape and with boundary intrusions and internal obstacles, such as islands.

A horizontal grid consisting of 23 by 28 points was generated by use of a grid generation program WESCORA for this study. Vertically 8 layers were used.

Model results were compared with field data at two stations. Station C were located in the middle of the lake. Station B was located in the western portion.

Time series of wind stress at Station C show that the wind field is temporarily varying. Therefore, spatially and temporarily varying wind stress field was used for the simulation. Time series of the wind stress field shows that there is a significant diurnal variation of wind speed(Fig. 4). Wind is calm early in the morning and strong in the afternoon and becomes calm again in the late night.

Currents at Station C are measured at Arms 1, 2 and 3, which are at the height of 17%, 33%,

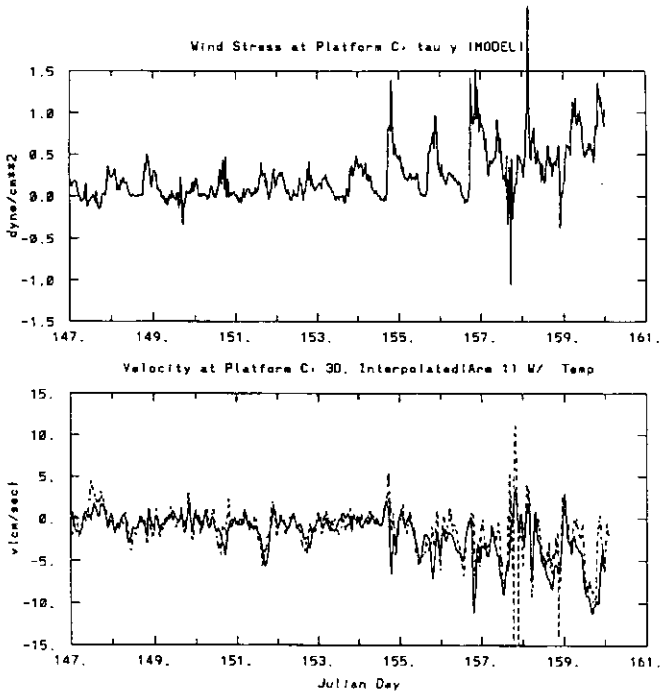

Fig. 5. Simulated (solid lines) and measured (dotted lines) currents at Station C (Arm 1: North-South direction)

and 78% of the total depth above the bottom, respectively. When the wind is light, the measured currents are usually small. As the wind increases in the afternoon, the surface currents follow the wind direction. However, when the wind speed reduces, the setup is released and the currents change the direction.

Therefore, general time history of measured currents have two peaks: a positive peak when the flow is from west to east during increasing easterly wind and a negative peak when the flow is from east to west during decreasing easterly wind.

Simulated results faithfully show the general trends of data as well as peaks(Figs. 4 and 5).

Wind direction at Station B is mainly toward the west during the two weeks. Measured currents at both arms show that the direction is toward the southwest. Arm 1 was at 16% of the total depth above the bottom. The average current at arm 1 is 3 cm/sec. A comparison of the model results with field data at arm 1 shows that the directions agree well. As shown in Figs. 6 and 7, the model could simulate the time of peak currents well. There is a discrepancy of approximately 1 cm/sec between the simulated and measured average currents. Considering the accuracy of current meters, this difference is considered negligible. However, the peak values of model currents are somewhat smaller than the field data, as it was found for Station C.

Arm 2 was at a height of 75% of the total depth. A comparison of the model current with field data at arm 2 shows generally good agreement in current direction over two weeks.

Model currents are somewhat stronger than the field data. The agreement between the model currents and field data in the north-south

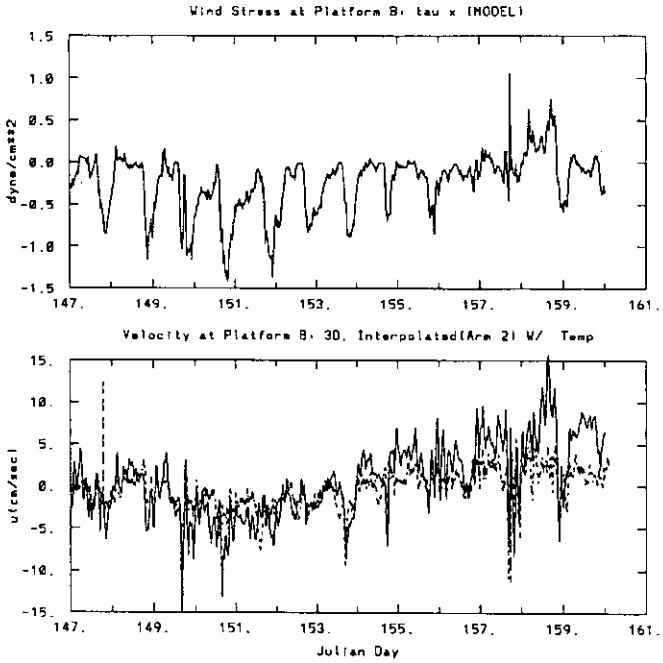

Fig. 6. Simulated (solid lines) and measured (dotted lines) currents at Station B (Arm 2: East-West direction)

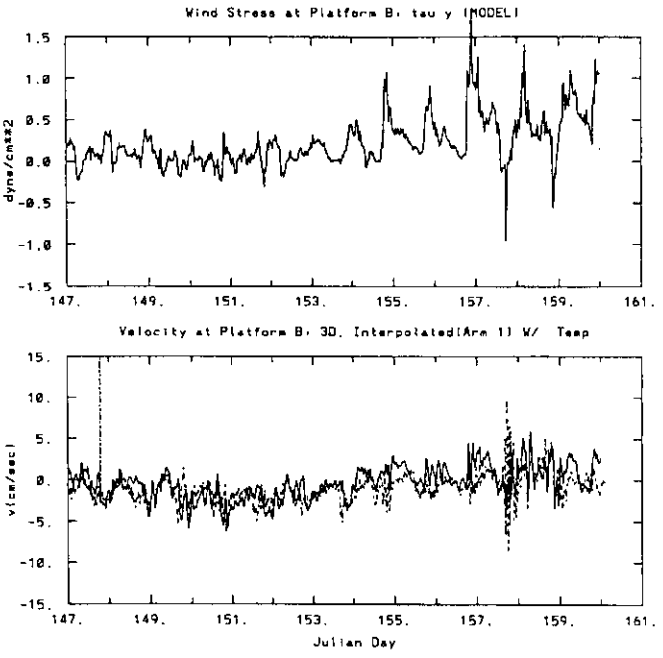

Fig. 7. Simulated (solid lines) and measured (dotted lines) currents at Station B (Arm 1: North-South direction)

direction becomes worse after Julian Day 154. Considering that the wind becomes strong in the north-south direction, the field data remains from north to south.

This seems to indicate that data have drifting problems. Both the measured and simulated currents at Station B indicate that flow is generally in the southwest-northeast direction, which is parallel to the boundary between the vegetation and the open water.

5. CONCLUSION

The effect of vegetation was parameterized as increased profile drag on the flow. To represent the vegetation distribution accurately, the concept of "equivalent vegetation density" is introduced. To simulate the flow in the littoral zone, momentum equations in the two layer system were derived and incorporated into CH3D (three-dimensional curvilinear-grid model) code.

CH3D was used to study the wind-driven circulation during the period of May 27, 1989, to June 10, 1989, in Lake Okeechobee to simulate the currents driven by winds. Both the simulated and measured currents in the vicinity of the vegetation zone were found to be primarily in the direction parallel to the vegetation boundary, thus suggesting relatively little transport across the vegetation boundary.

ACKNOWLEDGEMENT

Financial support provided by the South Florida Water Management District, West Palm Beach, Florida, U.S.A., through the Lake Okeechobee Phosphorus Dynamics Project is appreciated.

REFERENCES

Lee,Hye Keun. (1993). *Wind-Driven Circulation in Lake Okeechobee: The Effects of Thermal Stratification and Aquatic Vegetation, Ph*.D. Dissertation, Department of Coastal and Oceanographic Engineering, University of Florida, Gainesville,FL.

Roig, L.C. and King, I.P. (1992). "Continuum model for flows in emergent marsh vegetation." *Estuarine and Coastal Modeling*, Tampa, U.S.A., pp. 268-279.

Saville, T. (1952). *Wind set-up and waves in shallow water.* Technical Memorandum No. 27, Beach Erosion Board, Office of the Chief of Engineers, Corps of Engineers.

Sheng, Y. P. (1982). "Hydraulic applications of a second-order closure model of turbulent transport.", *Proceedings 1982 ASCE Hydraulic Division Specialty Conference on Applying Research to Hydraulic Practice*, Jackson, MS., pp. 106--119.

Sheng, Y. P., and Lee, H. K. (1991). *Computation of phosphorus flux between the vegetation area and the open water in Lake Okeechobee.* Report No. UFL/COEL – 91 - 022}, Coastal and Oceanographic Engineering Department, University of Florida, Gainesville, FL.

Whitaker, R. E.,Reid, R. O., and Vastano, A. C. (1975). *An analysis of drag coefficient at hurricane windspeeds from a numerical simulation of dynamical water level changes in Lake Okeechobee, Florida.* Technical Memorandum No. 56, Coastal Engineering Research Center, Corps of Engineers.

Hye Keun Lee, Water Resources Research Institute, Korea Water Resources Corporation, 462-1 Jonmin-Dong, Yusung-Gu, Taejon, 305-390 Korea.
(E-mail:hklee@kowaco.or.kr)

(Received October 5, 2000; accepted October 16, 2000)